5-18-2017

Building and Validating a Model for Investigating the Dynamics of Isolated Water Molecules

Grant Cates
Linfield College

Building and Validating a Model for Investigating the Dynamics of Isolated Water Molecules

G. W. Cates

A THESIS

Presented to the Department of Physics
LINFIELD COLLEGE
McMinnville, Oregon

In partial fulfillment of the requirements
for the Degree of

BACHELOR OF SCIENCE

May, 2017

THESIS COPYRIGHT PERMISSIONS

Please read this document carefully before signing. If you have questions about any of these permissions, please contact the DigitalCommons Coordinator.

Title of the Thesis:

Building & Validating a Model for Investigating the Dynamics of Isolated Water Molecules

Author's Name: (Last name, first name)

Cates, Grant

Advisor's Name

Crusser, Michael

DigitalCommons@Linfield is our web-based, open access-compliant institutional repository for digital content produced by Linfield faculty, students, staff, and their collaborators. It is a permanent archive. By placing your thesis in DigitalCommons@Linfield, it will be discoverable via Google Scholar and other search engines. Materials that are located in DigitalCommons@Linfield are freely accessible to the world; however, your copyright protects against unauthorized use of the content. Although you have certain rights and privileges with your copyright, there are also responsibilities. Please review the following statements and identify that you have read them by signing below. Some departments may choose to protect the work of their students because of continuing research. In these cases, the project is still posted in the repository but content will only be accessible by individuals who are part of the Linfield community.

CHOOSE THE STATEMENT BELOW THAT DEFINES HOW YOU WANT TO SHARE YOUR THESIS. THE FIRST STATEMENT PROVIDES THE MOST ACCESS TO YOUR WORK; THE LAST STATEMENT PROVIDES THE LEAST ACCESS.

X I **agree** to make my thesis available to the Linfield College community and to the larger scholarly community upon its deposit in our permanent digital archive, DigitalCommons@Linfield, or its successor technology. My thesis will also be available in print at Nicholson Library and can be shared via interlibrary loan.

OR

_____ I **agree** to make my thesis available **only** to the Linfield College community upon its deposit in our permanent digital archive, DigitalCommons@Linfield, or its successor technology. My thesis will also be available in print at Nicholson Library and can be shared via interlibrary loan.

OR

_____ I **agree** to make my thesis available in print at Nicholson Library, including access for interlibrary loan.

OR

_____ I **agree** to make my thesis available in print at Nicholson Library only.

Updated April 2, 2012

NOTICE OF ORIGINAL WORK AND USE OF COPYRIGHT-PROTECTED MATERIALS:

If your work includes images that are not original works by you, you must include permissions from original content provider or the images will not be included in the repository. If your work includes videos, music, data sets, or other accompanying material that is not original work by you, the same copyright stipulations apply. If your work includes interviews, you must include a statement that you have the permission from the interviewees to make their interviews public. For information about obtaining permissions and sample forms, see http://copyright.columbia.edu/copyright/permissions/.

NOTICE OF APPROVAL TO USE HUMAN SUBJECTS BY THE LINFIELD COLLEGE INSTITUTIONAL RESEARCH BOARD (IRB):

If your research includes human subjects, you must include a letter of approval from the Linfield IRB. For more information, see http://www.linfield.edu/irb/.

NOTICE OF SUBMITTED WORK AS POTENTIALLY CONSTITUTING AN EDUCATIONAL RECORD UNDER FERPA:

Under FERPA (20 U.S.C. § 1232g), this work may constitute an educational record. By signing below, you acknowledge this fact and expressly consent to the use of this work according to the terms of this agreement.

BY SIGNING THIS FORM, I ACKNOWLEDGE THAT ALL WORK CONTAINED IN THIS PAPER IS ORIGINAL WORK BY ME OR INCLUDES APPROPRIATE CITATIONS AND/OR PERMISSIONS WHEN CITING OR INCLUDING EXCERPTS OF WORK(S) BY OTHERS.

IF APPLICABLE, I HAVE INCLUDED AN APPROVAL LETTER FROM THE IRB TO USE HUMAN SUBJECTS.

Signature Grant Cates Date 18 May 17

Printed Name Grant Cates

Approved by Faculty Advisor [signature] Date 5/18/17

Updated April 2, 2012

Thesis Acceptance

Linfield College

Thesis Title: Building and Validating a Model for Investigating the Dynamics of Isolated Water Molecules

Submitted by: G.W. Cates Date Submitted: May, 2017

Thesis Advisor: _____

Dr. Michael Crosser

Physics Department: _____

Dr. Jennifer Heath

Physics Department: _____

Dr. Joelle Murray

ABSTRACT

Building and Validating a Model for Investigating the Dynamics of Isolated Water Molecules

Understanding how water molecules behave in isolation is vital to understand many fundamental processes in nature. To that end, scientists have begun studying crystals in which single water molecules become trapped in regularly occurring cavities in the crystal structure. As part of that investigation, numerical models used to investigate the dynamics of isolated water molecules are sought to help bolster our fundamental understanding of how these systems behave. To that end, the efficacy of three computational methods—the Euler Method, the Euler-Aspel Method and the Beeman Method—is compared using a newly defined parameter, called the *predictive stability coefficient* ρ. This new parameter quantifies each algorithm's stability such that the Euler-Aspel Method is determined to be relatively the most stable. Finally, preliminary results from investigating interactions between two dipole neighbors show that the computational tools that will be used for future investigations have been programmed correctly.

Contents

List of Figures

List of Tables

Chapter 1

Introduction

Water is one of the most ubiquitous substances on our planet. It is rather counterintuitive, then, how much remains to be understood about the basic properties of water. Many people are familiar with the general shape of water molecules, namely a Mickey Mouse head, consisting of two hydrogen "ears" and one oxygen "face". This geometry causes one end of the molecule to be more positively charged, while the other end is more negatively charged–a distribution known as a permanent dipole moment (see Fig. 1.1b). In a water droplet, the hydrogen-oxygen bond interactions of different water molecules dominate the dipole interactions and cause water to clump together. However, advances in nanotechnology allow us to disrupt the bond arrangement found in bulk water and create new spatial arrangements that result in fundamentally new properties, effectively transforming the system into "novel matter". The properties become even more unexpected when bonds are interrupted locally, such as through confinement in nanocages. Our understanding of isolated water molecules in such systems is currently in its infancy and is the focus of this thesis.

Given the importance of water in our world, insights from this research are broadly applicable, but the area of greatest potential impact is in biology. Biological systems often create naturally occurring channels where individual water molecules traverse the system or interfaces where single molecules are participating in hy-

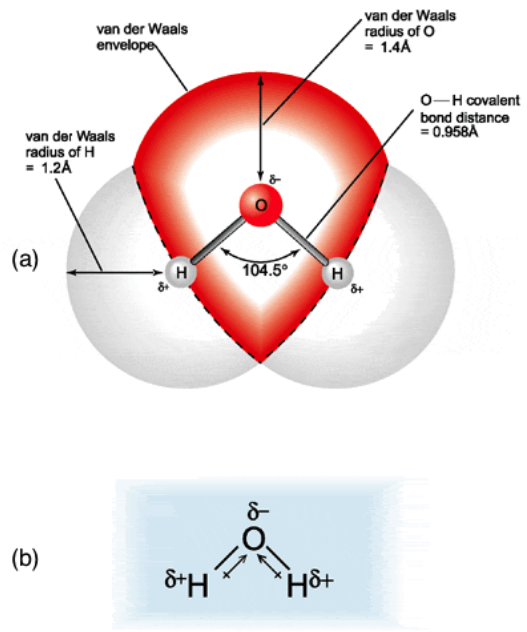

Figure 1.1: Properties of a water molecule are shown (a) as well as the distributfion of charge (b) (figure adapted from [1]).

drophilic/hydrophobic interactions, transcription and replication processes. If these bio-processes are to be truly understood, a fundamental understanding of confined water molecules and their resulting properties must be attained. The majority of current studies are done in biological systems, and any interpretation of the experimental results is obfuscated by the systems' complexity. Studies of simpler systems, then, are vital to gain insight into the fundamental mechanisms behind these biological processes.

Recently, *Dressel et. al* realized that a certain class of beryl crystals allowed for single water molecules to become trapped in naturally occurring cavities within the crystal structure. These naturally occurring cavities, or *nanocages*, are spaced in such a way that the dipoles are only able to interact via the dipole-dipole interaction[2]. It is believed that this system will provide evidence of incipient ferroelectricity in isolated water molecules for the first time and is currently the subject of intensive study[2]. As part of that study, computer models will be needed for proof-of-concept calculations, for verifying deduced understanding of the system and for investigating

regimes in which technology is yet able to touch. For instance, it may be technological impossible to measure the changing electric field of two dipoles interacting, but those electric fields can be modeled numerically.

To that end, a method for comparing stability (defined explicitly in Section 2.3.2) is provided and implemented on three algorithms for comparison—the Euler Method, the Euler-Aspel Method and the Beeman Method. Each algorithm, or computational engine, models the dynamics of a dipole rotating due to an external electric field. These results are then compared to expected results through frequency analysis so that stability may be quantified. Finally, the effects of nearest-neighbor interactions are briefly investigated.

Chapter 2

Background Theory

2.1 Introduction

Any computational model will rely on a collection of physical and computational theory. Presented first is the theory of dipoles according to Classical Electromagnetic Theory (CET). Then the Simple Pendulum is discussed, along with when it can, and cannot, model dipole dynamics. Finally, a brief overview of the Nyquist frequency and how it pertains to modeling oscillatory phenomena is given.

2.2 Physical Theory

2.2.1 What is a Dipole?

As discussed in Chapter 1 and depicted in Fig. 1.1, the geometry of a water molecule creates a separation of charge, which results in what is known as a permanent electric dipole, or *dipole* for short. Mathematically a dipole is defined as

$$\vec{p} \equiv \int \vec{r}\rho(\vec{r})dV \tag{2.1}$$

where $\vec{p}$ is the dipole moment, $\vec{r}$ is a position vector to the source charge, $\rho(\vec{r})$ is the charge distribution and the integral is taken over the total volume of the source.

From Eq. 2.1, the potential of the dipole is found to be

$$V_{dip}(\vec{r}) = \frac{1}{4\pi\epsilon_o}\frac{\vec{p}\cdot\hat{r}}{r^2} \tag{2.2}$$

where ϵ_o is the permittivity of free space, r is the magnitude of the measurement position vector and $\hat{r}$ is the direction of the measurement position vector. It is important to note that Eq. 2.2 is valid for a coordinate system in which the dipole is at the origin. Recalling that $\vec{E} = -\nabla V$, the electric field of the dipole $\vec{E}_{dip}$ is

$$\vec{E}(r,\theta) = \frac{p}{4\pi\epsilon_o r^3}(2\cos\theta\hat{r} + \sin\theta\hat{\theta}) \tag{2.3}$$

where θ is the angle the measurement position vector $\vec{r}$ makes with the xy-plane, and p is the magnitude of the dipole moment ($p = 6.1 \times 10^{-30}$ C $\cdot$ m for a water molecule[3]).

2.2.2 Dipole Dynamics

Consider a dipole in the xy-plane located at the origin with the only allowed degree of freedom being rotation about the z-axis. Now consider a constant external electric field $\vec{E}_{ext} = E_x\hat{x} + E_y\hat{y}$ applied to said dipole (see Fig. 2.1). The dipole will experience a torque $\vec{N}$ from the external electric field according to

$$\vec{N} = \vec{p} \times \vec{E}_{ext}. \tag{2.4}$$

Given the geometry of this system configuration, the torque will be entirely along the z-axis $\vec{N} = \pm N\hat{z}$ and have magnitude

$$N = pE\sin\theta \tag{2.5}$$

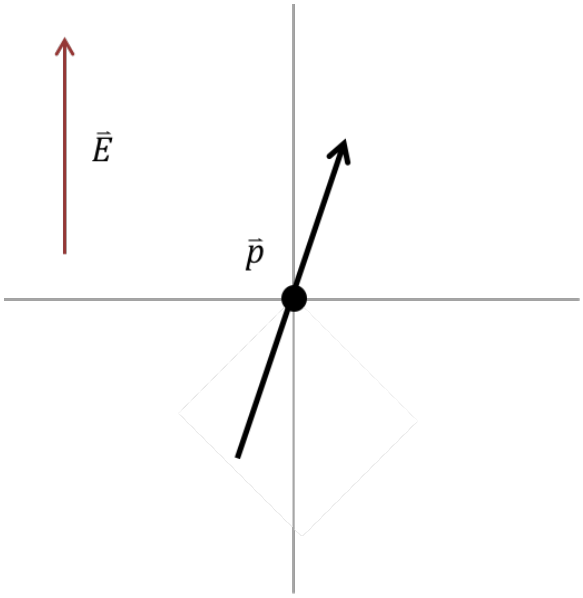

Figure 2.1: A single dipole is at the origin, with only one rotational degree of freedom allowed, and in the presence of an external electric field.

where $E = \sqrt{E_x^2 + E_y^2}$ is the magnitude of the external electric field and θ is the angle between $\vec{E}$ and $\vec{p}$.

Invoking Newton's Laws for rotational motion, the relationship for the angular acceleration $\ddot{\theta}$, moment of inertia I, dipole moment p and external electric field magnitude E can be found using Eq. 2.5.

$$\begin{aligned} I\ddot{\theta} &= pE\sin\phi \\ \ddot{\theta} &= \frac{pE}{I}\sin\theta \end{aligned} \tag{2.6}$$

Equation 2.6 represents the equation of motion (EOM) for the dipole. The EOM can also be found using the Lagrangian Method

$$\frac{\partial L}{\partial \theta} - \frac{d}{dt}\frac{\partial L}{\partial \dot{\theta}} = 0 \tag{2.7}$$

where the Lagrangian $L = T - U$ is the difference of the kinetic energy T and potential

energy U and $\dot{\theta}$ is the derivative of θ with respect to time t. For the system in Fig. 2.1,

$$T = \frac{1}{2} I \dot{\theta}^2 \tag{2.8}$$

$$U = -p \cdot E. \tag{2.9}$$

Combining Eqns. 2.8 & 2.9 with Eq. 2.7 yields

$$\ddot{\theta} + \sqrt{\frac{pE}{I}} \sin\theta \equiv \ddot{\theta} + \omega_o^2 \sin\theta = 0 \tag{2.10}$$

where ω_o is the characteristic frequency and $\ddot{\theta}$ represents the second derivative of θ with respect to time t. Equation 2.10 represents an oscillatory phenomenon not dissimilar to the pendulum.

2.2.3 The Pendulum

Oscillatory motion governed by Eq. 2.10 is widely studied in undergraduate physics courses. However, usually an approximating assumption is utilized to place the mathematics within reach of the students. That is, the oscillatory motion of a pendulum is studied within the small-angle approximation regime (SAAR); this system is sometimes referred to as the simple pendulum.

In the SAAR, $\theta \approx 0$ which allows for the approximation

$$\sin\theta \approx \theta. \tag{2.11}$$

As Fig. 2.2 shows, the relative error of the SAAR exceeds 1% when the initial angle $\theta_o = \theta_{max} > 0.244$ radians. For initial angles $\theta_o \leq \theta_{max}$, Equation 2.10 can be well-approximated as

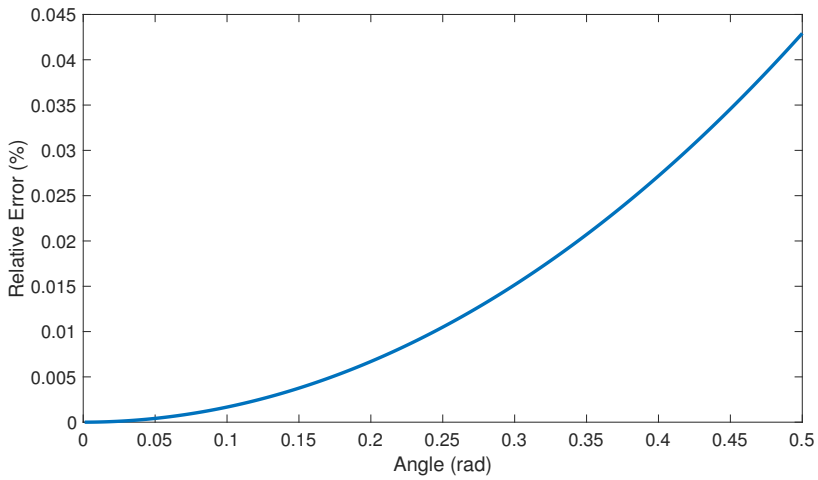

Figure 2.2: The relative error of the Small-Angle Approximation is given.

$$\ddot{\theta} + \omega_o^2 \theta = 0, \tag{2.12}$$

which has solutions of the form

$$\theta(t) = \theta_o \sin(\omega_o t + \phi) \tag{2.13}$$

where ϕ is some phase shift. Equation 2.11, however, strictly limits the systems Eq. 2.13 can describe; therefore, it is not conducive to studying the system of interest. To study such a system, the initial angle θ_o must not be limited to the SAAR.

Solving Eq. 2.10 exactly can be done [4, 5], but it requires integration techniques that are not usually taught in undergraduate mathematics courses (see [4] in particular for exact solutions). Such solutions show that the effects of nonlinearity become non-negligible outside of the SAAR, but for $\theta_o \leq 3\pi/4$ the nonlinearity manifests itself only in the sense that the angular frequency ω_o is a function of the initial angle θ_o [4]—this regime is referred to as the initial-angle dependent regime (IADR). Note, this also means that the period of oscillation T is dependent on the initial angle as well.

Additionally, Goldstein shows that the difference in the period due to nonlinearity

ΔT in the IADR is

$$\Delta T(\theta_o) = \frac{T_o}{4}\sin^2(\frac{\theta_o}{2}) \tag{2.14}$$

where $T_o = 2\pi\sqrt{\frac{I}{pE}}$ is the period found in the SAAR [6]. Equation 2.14 can be recast in terms of frequency, using the fact that $T = 2\pi/\omega$, as

$$\Delta\omega(\theta_o) = \frac{\omega_o \sin^2(\frac{\theta_o}{2})}{\sin^2(\frac{\theta_o}{2}) - 4}. \tag{2.15}$$

2.3 Model Stability

When attempting to model a continuous phenomenon in a discrete fashion, i.e. a temporally-dependent one, it is first necessary to determine appropriate values for parameters—such as an appropriate time step-size, or *timestep* τ—that yields stable results. Since there exists no general definition for what is a *stable result* nor a general methodology for determining when a parameter value is *appropriate*, it is often necessary to provide a definition for stability and develop a methodology that produces results which meet said definition.

One way to test model stability is to validate the results. In general, this can be done by comparing results to experimental ones, checking against one's expectation based on experience or comparing with analytic results.

2.3.1 An Example in Defining Stability

Consider the case of modeling the Earth's orbit around the Sun for one year; the Earth's final position from using different timesteps for a period of 1 year is depicted in Fig. 2.3. Note, the final position of the Earth is dependent on the timestep. For timesteps greater than or equal to 0.05 years, the model incorrectly predicts the final position of the Earth. Somewhere between 0.01-0.05 years, the model results become stable. Here, stability is defined as occurring when the Earth's final position equals

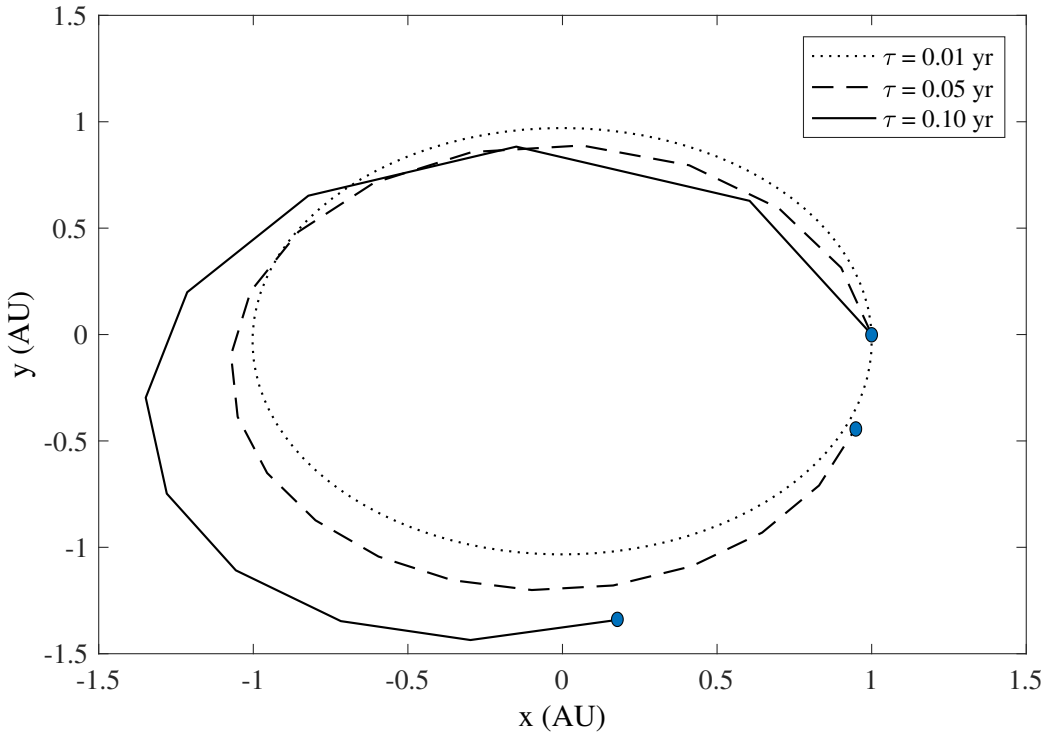

Figure 2.3: Figures showing examples of the variational principle when used to model Earth's orbit over one year. The orbits are predicted by using timesteps of 0.1, 0.05 and 0.01 years.

its initial position, which would be true assuming the Earth's orbit is closed.

A natural consequence of discretization, however, is that the final position will never *exactly* equal the initial position. Rather, as the timestep gets smaller the final position approaches the initial position. To quantify stability, a *convergence threshold* γ needs to be defined, such that when the magnitude of the difference between the final position and the initial position is less than or equal to γ the results are considered stable. More succinctly, the model results are considered stable if, and only if,

$$|\vec{r}_f - \vec{r}_i| \leq \gamma \tag{2.16}$$

where $\vec{r}_f$, $\vec{r}_i$ denote Earth's final and initial positions, respectively. The choice for γ largely depends on the accuracy required of the model by the experimenter.

2.3.2 Explicitly Defining Stability

For the purposes of modeling isolated water molecule dynamics, Equation 2.10 provides a quantitative way of defining stability. Namely, the relationship between frequency and external electric field is given by

$$\omega_o = \sqrt{\frac{pE}{I}}, \tag{2.17}$$

meaning frequency is proportional to the square-root of the external electric field magnitude. If an algorithm is able to reproduce this relationship for a range of electric fields, it will be considered stable. If not, the algorithm will be considered unstable for the purposes of modeling the dynamics of isolated water molecules. The method used to quantify stability is given in Section 3.3.1.

2.3.3 Oscillatory Phenomena and the Nyquist Frequency

Fortunately, when modeling oscillatory phenomena to probe system characteristics related to frequency, there exists a rigorous framework for defining stability via the Sampling Theorem:

Theorem 1 (The Sampling Theorem) *Let $f(t)$ be a bandlimited, continuous signal. Then f can be completely recovered when using a sample frequency $f_s \geq 2\omega_{max}$ where ω_{max} is the largest frequency of the system.*

Here, *bandlimited* simply means the system's frequency spectrum is finite and has a maximum characteristic frequency.

In practice, Theorem 1 states that when modeling a continuous phenomenon discretely, if the maximum frequency is known, a maximum timestep τ_{max} can be found according to

$$\tau_{max} = f_{s,min} = 2\omega_{max}. \tag{2.18}$$

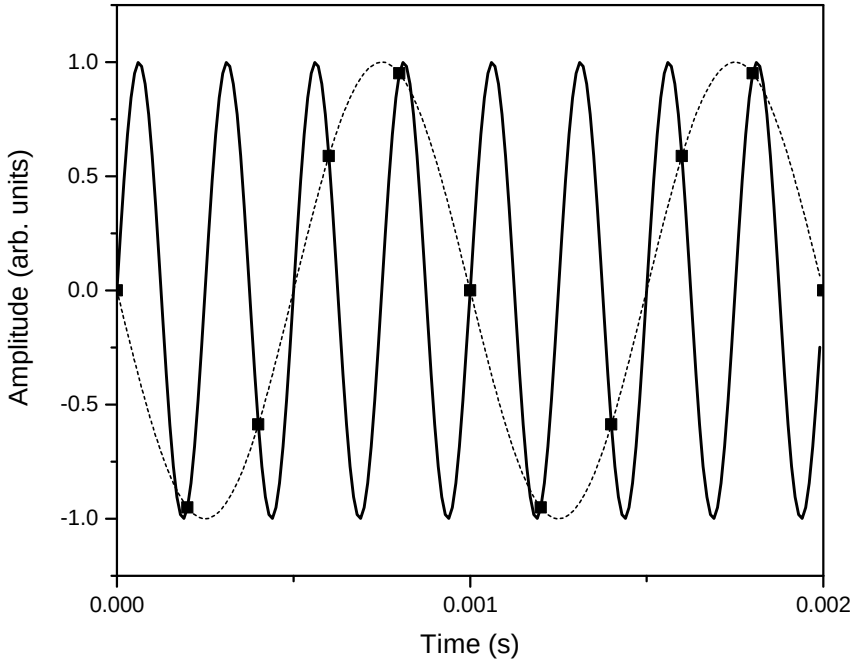

Figure 2.4: An example of aliasing that results from using a sample frequency that is too small. Here, a 5 kHz signal (solid line) is sampled at a rate of 4 kHz. The resulting alias frequency (dashed line) is 1 kHz.

This minimum sample frequency $f_{s,min}$ is known as the *Nyquist frequency* of the system. The Nyquist frequency is the smallest sample frequency that allows at least two measurements to be made per oscillation cycle, ensuring that aliasing does not occur when attempting to reconstruct the signal. An example of aliasing is given in Fig. 2.4. Here, a 5 kHz signal (solid line) is being sampled at a frequency of 4 kHz (denoted by the square points). When a best-fit is performed, the data suggests an incorrect signal frequency of 1 kHz (dashed line).

Even armed with the Nyquist frequency of a system, a model can still be inherently unstable depending upon the algorithm used. It is therefore important to test and validate the results of different algorithms.

Chapter 3

The Methods

3.1 Introduction

In order to determine which algorithms, or computational engines, yield stable results and in which regime, an experiment in which the outcome is already known must be designed. The results produced by each model can be compared to the expected results to determine whether or not that model's engine is stable and in which regime. First, however, the three algorithms being tested must be understood.

3.2 Computational Methods

By far, the most common engine used as an introduction into numerical modeling is the Euler Method (EM). The Euler Method, however, has well-known limitations when it comes to modeling oscillatory phenomena[7]. Therefore, the efficacy of the Euler-Aspel Method (EAM)—inaccurately referred to commonly as the Euler-Cromer Method[7]—and the Beeman Method (BM) is investigated.

The choices for selecting these two methods, as well as justification for the righteousness of the Euler-Aspel moniker, will be discussed below.

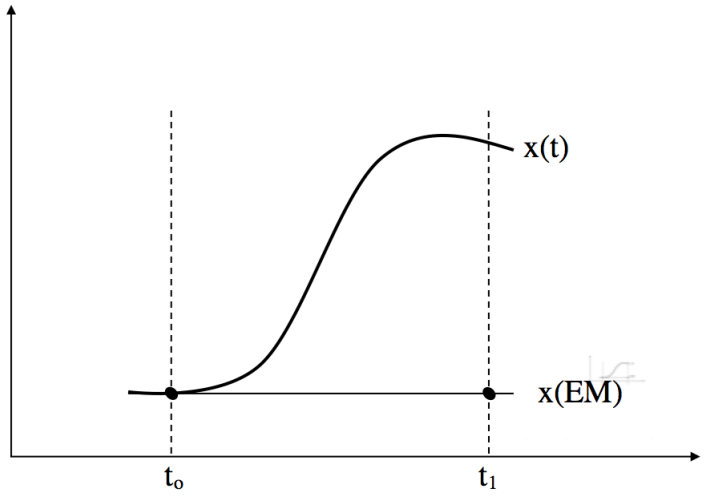

Figure 3.1: The position predicted by the Euler Method is compared to the analytic solution for some arbitrary function.

3.2.1 The Euler Method

The Euler Method (EM) is a procedure used in computational sciences to solve initial-value, first-order differential equations.

Consider the problem of modeling some system described by a function $x(t)$ known to be governed by the differential equation $\ddot{x} = f(x,t)$. Knowing some initial condition $x(t_o) = x_o$, the entire function $x(t)$ can be approximated using

$$t_i = t_{i-1} + \tau \tag{3.1}$$

$$v_i = v_{i-1} + f(x_{i-1}, t_{i-1})\tau \tag{3.2}$$

$$x(t_i) = x_{i-1} + v_{i-1}\tau \tag{3.3}$$

for velocity v_i and position x_i at some time t_i and for some timestep τ. Note, Eq. 3.3 is a linear approximation, and the variables x_i and v_i can be generalized.

An example of a single iteration of the EM used to approximate an arbitrary function is depicted in Fig. 3.1. Note the tangent line (shown in red) is built at

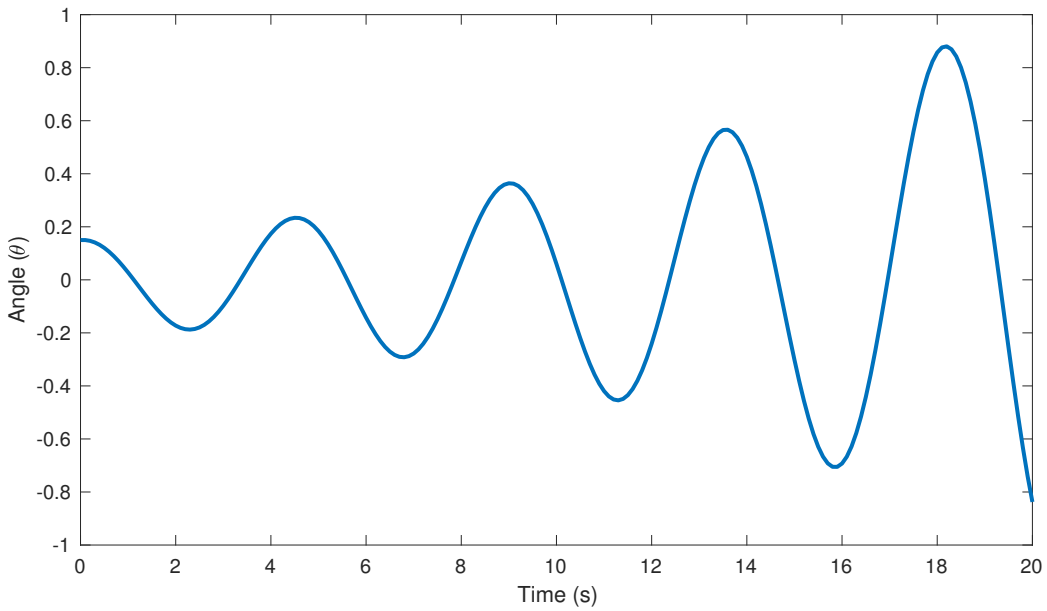

Figure 3.2: An example of the EM attempting to model a simple harmonic oscillator. Notice that the amplitude grows with each oscillation.

$x(t_o)$, and the subsequent point $x(t_1)$ is approximated to be a point on the tangent line determined by the timestep τ. It follows then, that as the timestep decreases, the accuracy in the prediction increases and converges to the actual function in the limit $\tau \to 0$.

The EM has well-known limitations when modeling oscillatory phenomena[7] as depicted in Fig. 3.2. Here, the results of modeling a simple harmonic oscillator are shown. The amplitude is predicted to grow as time increases, suggesting that energy is generated within the system as a function of time–violating conservation of energy. This error is attributed to the fact that the EM is a *first-point approximation* in that the next position is approximated using information from the beginning of the timestep, i.e. Eq. 3.3 utilizes v_{n-1}. As a result, the global error of the system grows without bound[**?**].

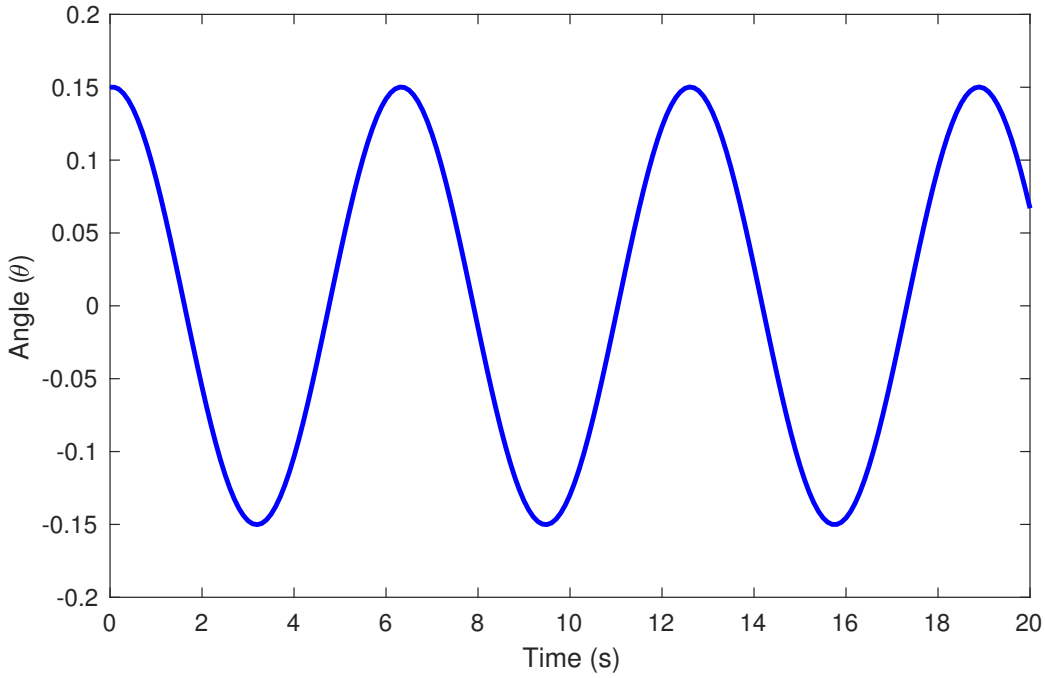

Figure 3.3: An example of the EAM attempting to model a simple harmonic oscillator.

3.2.2 The Euler-Aspel Method

A simple, and almost imperceptible, change to the EM solves the problem of conservation of energy and is called the Euler-Aspel Method (EAM). This is accomplished with a slight modification to Eq. 3.3, the approximation for x_i,

$$t_i = t_{i-1} + \tau \tag{3.4}$$

$$v_i = v_{i-1} + f(x_{i-1}, t_{i-1})\tau \tag{3.5}$$

$$x(t_i) = x_{i-1} + v_i\tau. \tag{3.6}$$

Note that Eq 3.6 now utilizes v_n—the value at the end of the timestep. For this reason, the EAM is sometimes referred to as a *last-point approximation*. The results of this change are shown in Fig. 3.3. As shown, the amplitude no longer grows with each iteration. Additionally, noting fewer peaks than the EM prediction, the EAM appears to predict a different frequency,

This method is commonly referred to incorrectly as the Euler-Cromer Method, presumably due to the paper Cromer published detailing this method and its effectiveness. However, in his paper he credits the discovery of this method to a Newton North High School student named Abby Aspel[7]. Recognizing the historical precedence of women not receiving their just recognition in academia, the method will henceforth be referred to as the Euler-Aspel Method.

3.2.3 The Beeman Method

The final algorithm investigated in this thesis is the Beeman Method (BM). The BM was chosen, because it was specifically designed to handle large systems with many interacting particles[8]. The BM runs according to

$$x_i = x_{i-1} + v_{i-1}\tau + \frac{\tau^2}{6}(4f(x_{i-1}, t_{i-1}) - f(x_{i-2}, t_{i-2})) \tag{3.7}$$

$$v_i = v_{i-1} + \frac{\tau}{6}(2f(x_i, t_i) + 5f(x_{i-1}, t_{i-1}) - f(x_{i-2}, t_{i-2})). \tag{3.8}$$

Notice, the BM is effectively making a prediction based upon the weighted average of information from the two previous timesteps. Additionally, the BM is not self-starting, so another algorithm—such as the EAM—needs to be used for the first calculation.

3.3 Experimental Methods

Now, an experiment is described which tests the efficacy of the aforementioned engines. To that end, consider the case of a water molecule confined to the origin in such a way that its dipole moment $\vec{p}$ is constrained to the xy-plane. That is,

$$\vec{p} = p_x\hat{x} + p_y\hat{y} + 0\hat{z} \tag{3.9}$$

Suppose the only allowed degree of freedomis rotation about the z-axis. Now, suppose the dipole is subject to a constant external electric field

$$\vec{E}_{ext} = E\hat{y} \tag{3.10}$$

as shown in Fig. 2.1. What effect would this have on the dipole?

According to Eq. 2.5, the dipole will experience a non-zero torque $\vec{N}$ assuming the angle $\theta \neq n\pi$ (for $n \in \mathbb{Z}$) where the angle is taken between $\vec{p}$ and $\vec{E}$. From Eq. 2.10, such a torque creates oscillatory motion according to

$$\ddot{\theta} + \omega_o^2 \sin\theta = 0 \tag{3.11}$$

where, again, ω_o is the characteristic frequency and

$$\omega_o = \sqrt{\frac{pE}{I}}. \tag{3.12}$$

Again, as described in Section 2.3.1, Equation 3.12 provides the desired test case for determining stability. By comparing the relationship between model-predicted frequencies and electric field with the expected frequencies and electric field, model stability can be quantified, as shown below.

3.3.1 Experimental Design

In order to predict the frequency of oscillation, first the dynamics of the dipole oscillating due to the external electric field for a total runtime R must be modeled. For ease of calculation, it is assumed that oscillating dipoles lose zero energy due to radiation. While this assumption is not based in reality, it still allows for the calculation of the desired quantity, namely frequency, because including dipole radiation would result in an attenuation of the amplitude without affecting the characteristic

frequency.

First, a total runtime R, a timestep τ, a set of initial angles for the dipole Θ and a set of electric field magnitudes $\mathbb{E}$ are determined (see Sec. 3.3.2). For each electric field magnitude $E_i \in \mathbb{E}$ and initial angle $\theta_k \in \Theta$ each model runs for R seconds. Then, the angular displacement versus time data are fit to the First-Order Fourier Series

$$\theta(t) = a_o + a_1 \sin \omega_k t + a_2 \cos \omega_k t \tag{3.13}$$

where $a_o, a_1, a_2 \in \mathbb{R}$ and ω_k is the predicted frequency for initial angle θ_k. After doing this for each $\theta_k \in \Theta$, a set of predicted frequencies Ω_{E_i} is created. Finally, the average predicted frequency $\langle \Omega_{E_i} \rangle = \omega_{E_i}$ and variance in said average σ_{E_i} is found. The datum point is taken to be

$$(E_i, \omega_{E_i} \pm \sigma_{E_i}). \tag{3.14}$$

The above process is repeated for the remaining $E_j \in \mathbb{E}$ (for $j \neq i$).

Once the average frequency for each electric field magnitude is determined, the average frequency versus electric field data are fit to the equation

$$f(x) = ax^n \tag{3.15}$$

where $a, n \in \mathbb{R}$. Since it is known (Eq. 3.12) that the frequency is proportional to the square-root of the electric field magnitude from, the models should produce data such that $n = 1/2$. This allows for the definition of the *predictive stability coefficient* as

$$\rho = |1 - \frac{n}{n_o}| \tag{3.16}$$

where $n_o = 1/2$. Note, this is an effective measure of how far off the model predicted frequencies are from the analytic result and provides a way to compare relative sta-

bility of different engines. For instance, if a set of k predictive stability coefficients is ranked, the model associated with ρ_o is more stable than the model associated with ρ_1 which is more stable than the model associated ρ_2 ... which is more stable than the model associated with ρ_k.

Ideally the model will have a predictive stability coefficient $\rho \ll 1$. Additionally, if a comparison between two ρ_i, ρ_j that are very close in value needs to be made, the predicted coefficient values can be compared to the accepted value $a = \sqrt{p/I}$.

3.3.2 Tuning the Parameters

There exist an infinite number of choices for the model's parameters: runtime R, set of electric field magnitudes $\mathbb{E}$, set of initial angles Θ and timestep τ. For some of the parameters a good choice may be obvious. For instance, the largest timestep that produces stable results is $\tau_{max} = 2\omega_o$ according to Theorem 1. For good measure, the timestep is taken to be $\tau = 0.01\tau_{max}$.

For the remaining parameters, well-informed guesses must be made. A total runtime $R = 50$ seconds was chosen largely because it seems like a good place to start. The total runtime sets the lower bound for $\mathbb{E}$, because MATLAB requires at least four data points to perform the Fourier fit (Eq. 3.13). The upper bound is determined by the computational time and experimenter's patience. These two factors give $\mathbb{E} = \{E_i : \log_{10} E_i = n \text{ for } n = -14, -13, ..., -5, -4\}$. Finally, the IADR ($\theta_o \leq 3\pi/4$) gives the set of initial angles Θ. The symmetry between the frequencies predicted by $\theta_i = -\theta_i$ and the angle of the external electric field ($\theta_E = \pi/2$) give $\Theta = \{\theta_i : \theta_i = 0.01\pi n \text{ for } -25 \leq n < 50\}$. Note, all the angles are given relative to the positive x-axis. Figure 3.4 shows the setup with the set of possible initial angles highlighted in purple. The symmetry occurs about the vertical axis.

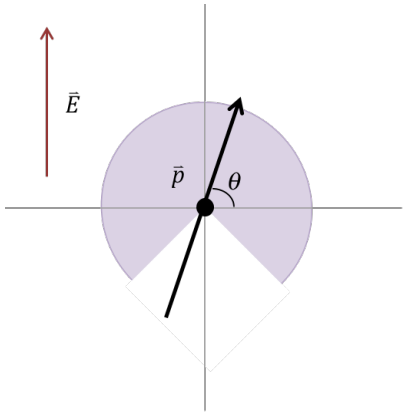

Figure 3.4: The setup for experimentation is shown again, with the addition of the possible initial angles (shown in purple).

Chapter 4

The Results and Analysis

4.1 Introduction

To analyze each engine's data, MATLAB's Curve Fitting Toolbox is used to fit each frequency versus external electric field data set to the power function

$$f(x) = ax^n \tag{4.1}$$

where the values of a and n are expected to be 56,000 and 0.5, respectively, from Eq. 3.12. Once the values for each have been determined, the predictive stability coefficient is determined. This calculation is followed with analysis of the aforementioned results, as well as preliminary results from the next step of investigation: how do dipoles interact with their nearest-neighbors.

4.2 Results and Analyses

Table 4.1 shows the results for each model when looking over the entire electric field range $\mathbb{E}$. Note, the values determined for the EM ($a = 0.16 \pm 0.65$ and $n = -0.01 \pm 0.17$) are no where near the expected values. This result is as expected since it is known that the EM has trouble modeling oscillatory phenomena. Somewhat

Table 4.1: The results of fitting each model's data sets are given for the full-range of electric field magnitudes.

Model	a	n	ρ
Actual	$56,000$	0.5	-
EM	0.16 ± 0.65	-0.01 ± 0.17	1.02
EAM	$54,000 \pm 3,900$	0.51 ± 0.01	0.02
BM	$4,400 \pm 3,200$	0.51 ± 0.01	0.02

surprisingly, the EAM and the BM produce the same predictive stability constant $\rho = 0.02$. While the BM method is supposed to provide more accurate predictions, it was built to do so for systems with a large number of interacting particles. It may be, then, that the extra predictive stability of the BM does not manifest until larger systems are analyzed. Note, however, the EAM better predicts the constant of proportionality $a = \sqrt{p/I}$, while the BM under-estimates the value. Technically, since only information about the relationship between frequency and external electric field is desired, the discrepancy in predicting this value is negligible. However, considering the fact that the BM method is more computationally expensive, it is determined that the EAM is the more efficient and more reliable engine.

Table 4.2: The results of fitting each model's data sets are given for the limited-range of electric field magnitudes $10^{-13} \leq E \leq 10^{-9}$ N/C.

Model	a	n	ρ
Actual	$56,000$	0.5	-
EM	$4,500 \pm 6,200$	0.40 ± 0.07	0.20
EAM	$45,000 \pm 7,700$	0.50 ± 0.01	0.01
BM	$38,000 \pm 3,200$	0.50 ± 0.01	0.01

When examining the raw data, it appears that the EM becomes a more viable candidate in the range $10^{-13} \leq E \leq 10^{-9}$ N/C. Table 4.2 provides the results from similar analyses for this limited electric field magnitude range. In this range, the EM is relatively more stable than it is in the full range and predicts a better constant of proportionality, but the error in the latter has increased significantly. Addition-

ally, the EAM and BM both have a slightly better predictive stability coefficient, but their predictions for the constant of proportionality a both are less accurate from the expected value. It appears possible that the EM may become a viable candidate when the external electric field is very weak ($E \ll 10^{-14}$ N/C), but to test this, the total runtime must be increased due to the minimum number of data point requirements imposed by MATLAB's curve fitting toolbox. Considering the runtime for the larger electric field magnitude—on the order of days for each—this investigation is postponed until access to more computing power is made available.

4.3 Reproducibility

While attempting to reproduce the above results, the same experimental methods were followed. However, given the same initial conditions, different average frequencies with different variances were predicted. Figure 4.1 is a typical representation of the relationship between average frequency with variance versus number of iterations. Notice that the average frequency and variance both asymptotically approach some value.

Initially, it appears this suggests some error in the code, where some type of data carry-over occurs between iterations. However, after Rubber Duck Debugging the model, no instance of data carry-over was detected. For good measure, an attempt was made to reproduce the results where MATLAB's memory was cleared between each iteration, yet the same behavior resulted. Even when MATLAB is closed and reopened between iterations, the machine's memory is cleared between iterations and the model is run on a different machine, this same behavior in results persists.

A possible candidate for this behavior is round-off error. MATLAB has a fixed number of decimal places—by default, 16—for which precision is guaranteed. The values used for calculation in the above models flirt with, and sometimes exceed, this threshold. Assuming MATLAB has some regular method of handling decimal

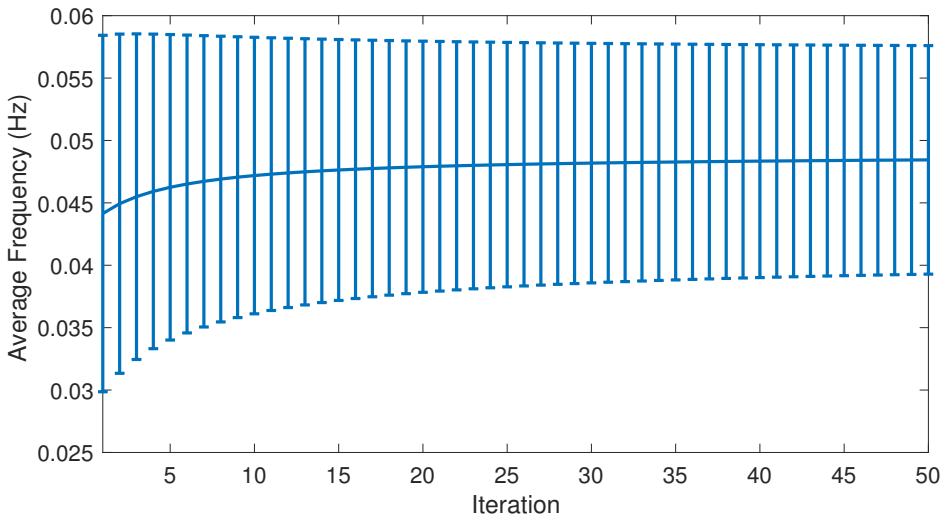

Figure 4.1: A typical example of the results of trying to reproduce the average frequency with variance for a given electric field magnitude. Both the predicted average frequency and variance in the average quickly converge.

precision, it is possible that this is responsible for the lack of exact reproducibility. It is possible to increase the decimal precision, but this also increases the computational cost. As such, investigations on this front are postponed until access to greater computing power exists.

Even without pinpointing the exact causation, there is little reason to believe that this reproducibility variation significantly affects the overall analysis. As Fig. 4.1 suggests, the difference between the convergent value and initial value is small. If anything, running multiple iterations for each electric field magnitude will result in more accurate approximations for a and n, and therefore more desirable predictive stability coefficients. Again, all of these assumptions can be tested once access to greater computing power is granted.

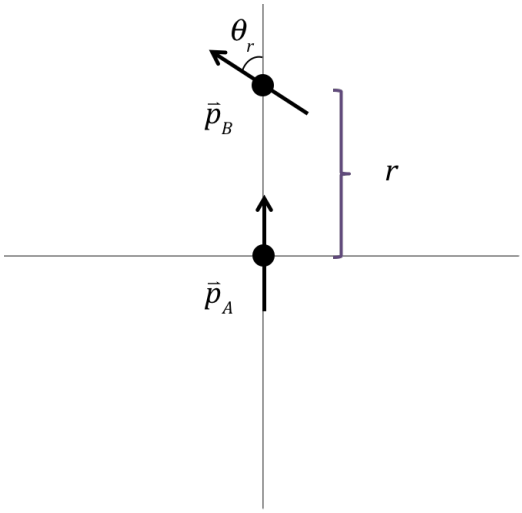

Figure 4.2: Two dipoles, one at the origin and one a distance r away on the vertical axis, are shown starting with a relative initial angle θ_r between them.

4.4 Interacting Neighbors: Preliminary Results

4.4.1 The Experimental Setup

To determine the effect of a nearest-neighbor, a dipole is added to our original system and is located at $(0, r)$. The dipoles are given a relative initial angle $\theta_{ro} = |\theta_{Bo} - \theta_{Ao}|$ where θ_{Ao}, θ_{Bo} are the initial angles of Dipole A and Dipole B, respectively, and are measured relative to the positive x-axis (see Fig. 4.2). Using the EAM, the motion of the dipoles is then modeled with the only external electric field originating from the nearest-neighbor using the parameter values in Table 4.3.

Table 4.3: The values for each parameter used for investigating the effects of one nearest-neighbor interaction are given.

Parameter	Variable	Value
Runtime	R	50
Timestep	τ	0.05
Separation Distance	r	1×10^{-10}
Dipole A Initial Angle	θ_{Ao}	0.5π
Relative Initial Angle	θ_{ro}	0.01π

4.4.2 Preliminary Results & Semi-Qualitative Analysis

Figure 4.3 suggests that two dipoles in this configuration will exhibit behavior similar to windshield wipers moving in opposite directions. Initially, Dipole A's positive side attraction to Dipole B's negative side causes Dipole A to experience a negative torque and begin rotating to the right. For similar reasons, Dipole B experiences a positive torque and begins rotating to the left. In other words, both dipoles are rotating towards $3\pi/2$ from opposites directions. As they both approach $3\pi/2$, their angular momentum is fighting the repelling Coulomb force from their like-charged sides. Note, Dipole A does not quite make it to $3\pi/2$ (or, equivalently roughly -1.57), while Dipole B rotates slightly beyond $3\pi/2$ (or, equivalently roughly 4.712). Lastly, using MATLAB's Curve Fitting Toolbox, the frequency of oscillation is found to be $f = 0.367$ Hz.

These results match expectation when the initial angles of each dipole is considered, in addition to the interaction of (un)like charges according to the Coulomb interaction.

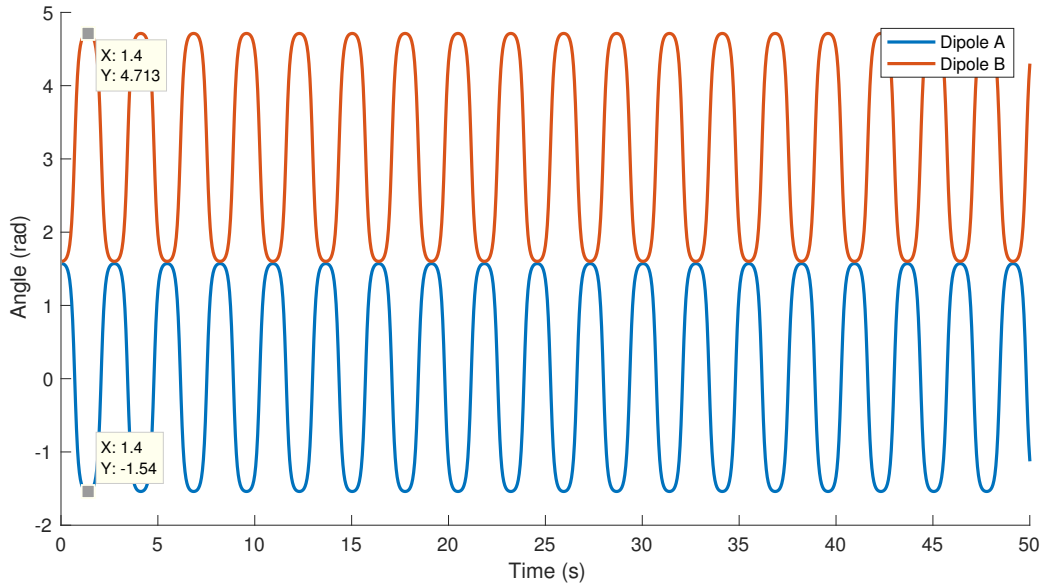

Figure 4.3: Preliminary results from modeling nearest-neighbor interactions are given. The dipoles initially oscillate away from each other. As they both approach $\theta = -\pi/2$ from opposite directions, they begin to repel each other until they both reverse direction.

Chapter 5

The Conclusion and Future Work

5.1 Drawing Conclusions

For the range of electric fields probed, ($E = 10^{-14}$ to 10^{-4} N/C), the EAM is the superior algorithm of the three. When compared to the EM method, in both the full and limited ranges, the predictive stability coefficient is significantly more desirable (1.02 vs 0.02 and 0.20 vs. 0.01, respectively). When compared to the BM, although they have the same predictive stability coefficient, the EAM better predicts the value for the coefficient $a = \sqrt{p/I} \approx 56,000\ \sqrt{C/(kg \cdot m)}$ than the BM ($45,000 \pm 7,700$ vs. $38,000 \pm 7,500$, respectively). It is slightly surprising that the BM is not more accurate, but this may be because the benefits of using the BM emerge when studying large systems with many interacting particles. After all, it was designed to thrive in such scenarios. Many of these calculations should be carried out with more computing power than the personal machine used to perform these calculations offers. Parallelizing these computations across many computers is promising in the absence of a supercomputer.

The preliminary results in Fig. 4.3 suggests that the computational tools developed to consider nearest-neighbor interactions is working as expected. This will serve as the background for the work moving forward.

5.2 Looking Ahead

There exists multiples avenues from the conclusion of this thesis for future research. First and foremost, more regimes need to be tested for stability. Not only do electric field strengths outside of those tested need to be investigated, but the effects of runtime on stability should be tested as well. For one, even from the cursory results in Figs. 3.2 & 3.3, it is obvious that different predictions for frequency are made by noting fewer number of peaks in the latter than the former. Secondly, the decrease in the EM's predictive stability coefficient from $\rho = 1.02$ to $\rho = 0.20$ suggests that there may be a limited range in which the EM is more effective. By learning more conclusively how electric field strength and total runtime affect stability, each model can be selectively employed for an appropriate range of systems.

Now that two dipoles are interacting, systems with different geometric arrangements of neighbors can be investigated. For instance, how does a rectilinear arrangement (i.e. neighbors at north, south, east, west) affect the dynamics of a dipole compared to a hexagonal arrangement (i.e. a dipole at the center of a hexagon)? Furthermore, how does the intermolecular spacing affect the dynamics? (Most likely this effect is similar to reducing the external electric field acting on a single dipole.) What happens when the order of nearest-neighbor interactions is increased? That is, instead of being influenced only by the nearest-neighbors, the dipole interacts additionally with its neighbor's nearest-neighbors.

Lastly, in hopes of finding signatures of ferroelectricity, more realistic behavior needs to be incorporated into the model. For example, dipole radiation is completely ignored in the model thus far. Additionally, any induced magnetic fields or potential magnetic interactions are currently ignored as well. Incorporating these phenomena may be necessary to capturing ferroelectric behavior.

References

[1] `http://higheredbcs.wiley.com/legacy/college/boyer/0471661791/reviews/pH/ph_water.htm`

[2] M. Dressel, B. Goshunov, *Broad-band optical spectroscopy of low-energy excitations of water molecules confined in nano-cage of bery crystal lattice*, preprint 2016.

[3] D. Griffiths, *Classical Mechanics*, Addison-Wesley, 1988.

[4] A. Belendez, C. Pascual, D.I. Mendez, T. Belendez and C. Neipp, *Exact solutions for the nonlinear pendulum*, Revista Brasileira de Ensino de Fisica (29) (2007), 645–648.

[5] M. I. Qureshi, M. Rafat, S. Ismail Azad, *The exact equation of motion of a simple pendulum of arbitrary amplitude: a hypergeometric approach*, Eur. J. Phys. (31) (2010), 1485-1497.

[6] H. Goldstein, *Introduction to Electrodynamics: Fourth Edition*, Pearson, 2013.

[7] A. Cromer, *Stable solutions using the Euler approximation*, Am. J. Phys. (5) (1981), 455–459.

[8] D. Beeman *Some Multistep Methods for Use in Molecular Dynamics Calculations*, J. Comp. Phys. (20) (1976), 130-139.